UCSF
UC San Francisco Previously Published Works

Title

High Resolution 13C MRI with Hyperpolarized Urea: in vivo T2 Mapping and 15N Labeling Effects

Permalink

https://escholarship.org/uc/item/7s21481k

Journal

IEEE Transactions on Medical Imaging, 33(2)

ISSN

0278-0062

Authors

Reed, Galen D
von Morze, Cornelius
Bok, Robert
et al.

Publication Date

2014-02-01

DOI

10.1109/tmi.2013.2285120

Peer reviewed

High Resolution ^{13}C MRI With Hyperpolarized Urea: *In Vivo T_2 Mapping and ^{15}N Labeling Effects*

Galen D. Reed[*] **[Student Member, IEEE]**,
Radiology and Biomedical Imaging, University of California-San Francisco, San Francisco, CA 94143 USA

Cornelius von Morze,
Radiology and Biomedical Imaging, University of California-San Francisco, San Francisco, CA 94143 USA (cornelius.vonmorze@ucsf.edu)

Robert Bok,
Radiology and Biomedical Imaging, University of California-San Francisco, San Francisco, CA 94143 USA (robert.bok@ucsf.edu)

Bertram L. Koelsch,
Radiology and Biomedical Imaging, University of California-San Francisco, San Francisco, CA 94143 USA (bkoelsch@berkeley.edu)

Mark Van Criekinge,
Radiology and Biomedical Imaging, University of California-San Francisco, San Francisco, CA 94143 USA (mark.vancriekinge@ucsf.edu)

Kenneth J. Smith,
Department of Chemistry, University of San Francisco, San Francisco, CA 94117 USA (kensmith415@gmail.com)

Hong Shang,
Radiology and Biomedical Imaging, University of California-San Francisco, San Francisco, CA 94143 USA (hong.shang@ucsf.edu)

Peder E. Z. Larson [Member, IEEE],
Radiology and Biomedical Imaging, University of California-San Francisco, San Francisco, CA 94143 USA (peder.larson@ucsf.edu)

John Kurhanewicz, and
Radiology and Biomedical Imaging, University of California-San Francisco, San Francisco, CA 94143 USA (john.kurhanewicz@ucsf.edu)

Daniel B. Vigneron
Radiology and Biomedical Imaging, University of California-San Francisco, San Francisco, CA 94143 USA (dan.vigneron@ucsf.edu)

[*]corresponding author. galen.reed@ucsf.edu.

Abstract

^{13}C steady state free precession (SSFP) magnetic resonance imaging and effective spin-spin relaxation time (T_2) mapping were performed using hyperpolarized [^{13}C] urea and [^{13}C, ^{15}N$_2$] urea injected intravenously in rats. ^{15}N labeling gave large T_2 increases both in solution and *in vivo* due to the elimination of a strong scalar relaxation pathway. The T_2 increase was pronounced in the kidney, with [^{13}C, ^{15}N$_2$] urea giving T_2 values of 6.3±1.3 s in the cortex and medulla, and 11±2 s in the renal pelvis. The measured T_2 in the aorta was 1.3±0.3 s. [^{13}C] urea showed shortened T_2 values in the kidney of 0.23±0.03 s compared to 0.28±0.03 s measured in the aorta. The enhanced T_2 of [^{13}C, ^{15}N$_2$] urea was utilized to generate large signal enhancement by SSFP acquisitions with flip angles approaching the fully refocused regime. Projection images at 0.94 mm in-plane resolution were acquired with both urea isotopes, with [^{13}C, ^{15}N$_2$] urea giving a greater than four-fold increase in signal-to-noise ratio [^{13}C] over urea.

Keywords

Angiography; dynamic nuclear polarization; hyperpolarized; steady state free precession (SSFP); urea

I. Introduction

Magnetic resonance imaging with hyperpolarized ^{13}C-labeled compounds is a powerful tool for molecular imaging in preclinical research with clinical feasibility demonstrated [1]. In the dissolution dynamic nuclear polarization (DNP) experiment [2], the ^{13}C-enriched imaging probe is doped with millimolar amounts of an organic radical, cooled to solid state, and irradiated at the electron/nuclear transition frequencies in a high magnetic field. In this manner, nuclear polarizations as high as 70% have been reported [3], or more typically 10%–30%. This represents a gain of four orders-of-magnitude over the Boltzmann polarization at room temperature and high magnetic field. The solid state sample is rapidly dissolved with heated solvents while retaining the polarization into liquid state, creating a new class of injectable MRI contrast agents. The hyperpolarization of endogenous substrates enables minimally invasive monitoring of key specific metabolic pathways and transport processes *in vivo* [4]–[7] with demonstrated utility in oncological [1], [8]-[11] and perfusion [12]–[16] imaging.

Hyperpolarized MR angiography (MRA) and perfusion imaging have interesting properties differentiating them from conventional MRA methods. Unlike ^{1}H MRA which utilizes altered contrast of the water in blood vessels or perfused tissues from radio frequency (RF) preparation pulses, flow-encoding gradients, or the injection of relaxation agents, hyperpolarized ^{13}C magnetic resonance allows for direct imaging of the injected compound. Therefore, this method provides background free signal due to the low ^{13}C natural abundance (~ 1%) in tissues and the low gyromagnetic ratio (γ) of ^{13}C nucleus. This has enabled several intriguing applications including coronary angiography [15] and perfusion assessment within the brain [13], [14] kidney [16], and in preclinical cancer models [17].

Despite the unique advantages of hyperpolarized perfusion imaging, there are several drawbacks. Although the DNP process gives a four order of magnitude gain over Boltzmann polarization, high resolution imaging has been difficult for a number of reasons. First, ignoring the polarization increase, the voltage induced in the receiver coil by a magnetic moment μ will scale as, $\varepsilon \sim \mu\omega_0 \sim \gamma^2$, while the noise scales as γ. Therefore, the signal-to-noise ratio (SNR) gain from DNP is offset to some by the inherently low SNR from imaging a low γ nucleus. A second significant challenge is the gradient pulse area requirement for a given resolution, which scales as $1/\gamma$ and necessitates long encoding pulses on clinical MRI systems.

A novel solution to the resolution and SNR limitations is the use of a long T_2 probe in conjunction with acquisitions employing multiple refocusing pulses [13]. If T_2 is long compared to the imaging time, 180° refocusing RF pulses (preceded by a 90° excitation) are signal-optimal and offer very large SNR improvements. Previously designed hyperpolarized perfusion probes include (bis–1,1–(hydroxy–methyl)–1–^{13}C–cyclopropane–d_8) (sometimes abbreviated as HMCP or HP001) and tert butanol, both of which have T_2 values in the range of 1.4–4 s *in vivo* [13], [18]. Since this is greater than the phase encoding time for a single image, projection images can be acquired at 1 mm in-plane resolution with SNR comparable to ^{1}H MRI [13].

Another potential solution to the SNR and resolution limitations is the use of endogenous, non toxic imaging probes such as urea [12] which could potentially be injected in very high concentrations. Urea is a normal blood constituent produced by amino acid metabolism, and it is typically found with steady state concentrations of 5.5±2.0mM(33±12 mg/dL) in the blood of healthy humans [19] and rats [20]. Urea has been shown to be well-tolerated intravenously in very large doses even in patients with end stage renal failure on dialysis [21].

Although ^{13}C urea is one of the most promising angiographic imaging agents due to its low toxicity, image quality is limited by its comparatively short relaxation times. Scalar coupling of the ^{13}C to the fast-relaxing quadrupolar ^{14}N causes a large T_1 decrease at low fields leading to polarization loss during transport from the polarizer to the imaging magnet [22]. Furthermore, the T_2 range measured in this manuscript (0.09–0.30 s) is approximately an order-of-magnitude lower than that of typical ^{13}C compounds measured *in vivo* [13], [18], [23] and at least two orders-of-magnitude lower than those measured in aqueous solution.

In this study, we found that ^{15}N labeling the amide groups of [^{13}C] urea results in a 250 fold increase in the T_2 in aqueous solution. *In vivo* T_2 mapping experiments showed that [^{13}C, ^{15}N$_2$] urea still had a much longer T_2 than [^{13}C] urea, although the increases were highly spatially heterogeneous. This difference was most apparent in the kidneys, where T_2 values as high 11 ± 2 s were observed with [^{13}C, ^{15}N$_2$] urea. The measured T_2 of [^{13}C] urea was slightly lower in the kidneys than in the blood, with values of 0.231±0.026 and 0.279±0.027 s respectively. The large T_2 increases associated with ^{15}N labeling were utilized to extract large SNR gains via steady state free precession (SSFP) imaging with flip angles in the fully refocused regime. [^{13}C, ^{15}N$_2$] urea projection images depicted the kidney,

aorta, and iliac branches in great detail and gave a factor of 4 SNR improvement over [^{13}C] urea.

II. Theory

A. SSFP Signal Behavior

The signal behavior of the SSFP sequence applied to hyperpolarized nuclei has been described in detail previously [12], [13], [17], [24]–[26]. Typically, a $\theta/2$ preparation RF pulse is placed $TR/2$ before the first imaging repetition, and all pulses have alternating polarity. The flip angle θ tunes the degree of T_1 and T_2 weighing and the total image SNR [13], [24], [27], the latter of which is also highly dependent on the relaxation and sequence timing parameters. Assuming a small frequency spread, the analytic model derived by Svensson *et al.* giving the transverse magnetization at the nth phase encoding step can be used [13]

$$M_{xy,n} = M_{z,0} \; sin\frac{\theta}{2} \left[\left(E_1 \quad cos\frac{\theta}{2} \right)^2 + \left(E_2 \quad sin\frac{\theta}{2} \right)^2 \right]^{n/2} \quad (1)$$

where, $E_1 = \exp(TR/T_1)$, $E_2 = \exp(TR/T_2)$ The image SNR and pixel blurring can be calculated by

$$\text{signal} = max|h(x)| \quad (2)$$

$$\text{pixel width} = FWHM|h(x)| \quad (3)$$

with $h(x) = \text{FFT}\{M_{xy}\}$ is the point spread function in the phase encoded direction. The simulated signal and pixel width for [^{13}C] urea and [^{13}C, ^{15}N$_2$] urea is shown in Fig. 1 for various T_2 values measured later in this manuscript.

This model provides a rough estimate of the imaging SNR, since the actual SNR realized will depend also on the k space image and the k space ordering. For N_{PE} phase encodes and in the long the limit of T_1, $T_2 \gg N_{PE}TR$, the SSFP signal reduces to $N_{PE}M_0$ when $\theta = 180°$. In this case, the sequence is similar to the CPMG fast spin echo sequence with the signal given by 1 giving a pure T_2 decay. With T_2 values less than the imaging time $N_{PE}TR$, a lower value of θ will provide a higher total signal and tighter point spread function. In this regime, signal dropout occurring at $\pm 1/2TR$ off resonance must also be considered. This effect is simulated in Fig. 2 ignoring relaxation. Clinical MRI systems generally have much stricter requirements on peak gradient amplitude, gradient switching rate, and RF pulse amplitude than high resolution systems designed for animal use. This creates challenges encoding large image matrices with low gyromagnetic ratio (γ) nuclei. Particularly, the TR used for high resolution imaging of low γ nuclei (15 ms for most experiments in this study) was much larger than values used previously for hyperpolarized SSFP on animal systems or for ^{1}H on clinical systems. This creates a significant challenge for imaging short T_2 compounds since at low flip angles and large TR values, the signal-loss banding occurs close to the resonant frequency.

B. Urea Transverse Relaxation

In solution, the measured ^{13}C transverse relaxation rate $R_2 = 1/T_2$ will be the sum of several pathways of varying strength

$$R_2 = R_{2,SC} + R_{2,CSA} + \sum_X R_{2,CXdd}. \quad (4)$$

$R_{2,CXdd}$ is the dipolar relaxation from nucleus X, which, for the ^{13}C label of urea, will be primarily from the four amide protons. The ^{15}N labeled compound will also have some dipolar contributions from the neighboring nitrogens. $R_{2,CSA}$ is the chemical shift anisotropy contribution which emanates from the variation in Larmor frequency experienced by the carbonyl ^{13}C during molecular tumbling. $R_{2,SC}$ is the pathway which arises from scalar coupling to a fast relaxing (usually quadrupolar) nucleus.

This scalar coupling of the second kind effect was recently shown to attenuate the low-field T_1 of [^{13}C] urea at low B_0 due to the strong ^{13}C–^{14}N scalar coupling constant (14 Hz) and fast ^{14}N relaxation time ($T_{1,N} \sim T_{2,N} \sim 1$ ms) [28]. This T_1 attenuation becomes negligible at high fields. However, the scalar relaxation pathway affects the T_2 even at high fields [29]

$$R_{2,SC} = \frac{4}{3}\pi^2 J^2 S(S+1)\left(\frac{1}{R_{1,N}} + \frac{R_{2,N}}{R_{2,N}^2 + \Delta\omega^2}\right). \quad (5)$$

Here, $\omega = \omega_C - \omega_N$ is the difference in Larmor frequency between the ^{13}C and ^{14}N nuclei, J is the coupling constant in Hz, S is the nuclear spin of ^{14}N. At 3T, the right-hand term in (5) is negligible since $\omega = 2\pi \times 22$ MHz, and $R_{2,N} \approx 1$ kHz [22], [28]. The left-hand term in the parentheses persists at high fields. This interaction has been used to indirectly estimate the relaxation times of halogens and other quadrupolar nuclei whose relaxation times are difficult to measure directly due to extremely broad line widths [30], [31]. This is possible since $R_{2,SC}$ scales as $1/T_1$ of the quadrupolar nucleus, so the latter parameter can be estimated if the coupling constant is known. Finer *et al.*. used line broadening due to $R_{2,SC}$ of the amide protons to estimate the rotation correlation time τ of urea in dilute solution [28]. In an identical manner, the ^{13}C scalar coupling relaxation can be derived by substituting the nitrogen quadrupolar relaxation term $R_{1,N} = \omega_Q^2 \tau$ the ^{14}N nuclear spin $S = 1$, and summing contributions from both nitrogens giving

$$R_{2,SC} = \frac{16\pi^2 J^2}{3\omega_Q^2 \tau}. \quad (6)$$

The ^{13}C T_2 due to the scalar coupling effect increases with increasing correlation time τ.

The dipolar and CSA terms can be expressed as

$$R_{2,CSA} + \sum_X R_{2,CXdd} = (\alpha_{CSA} + \alpha_{CHdd} + \alpha_{CNdd})\tau. \quad (7)$$

This model assumes the extreme narrowing limit of the spectral density function

$(2/5)\,\tau/\left(1+\omega_0^2\tau^2\right) \sim (2/5)\,\tau$. At $B_0 = 3$ T and using $\tau = 5$ ps estimated in [28] for urea in dilute solution at 17 °C, the product $\omega_0\tau = 10^{-3}$. The, a_{CSA}, a_{CHdd} and a_{CNdd} terms are the relative strengths of each pathways (in s^{-2}). ^{15}N labeling effectively replaces the $R_{2,SC}$ term in (4) and (6) with a dipolar term $R_{2,CNdd}$ from (7). The latter pathway is much weaker, and we found the solution aqueous solution T_2 of [^{13}C, ^{15}N$_2$] urea (24 ± 4 s) to be at least a factor of 200 greater than that of [^{13}C] urea (0.090±.014 s) at 25 °C. From (6), substituting $J = 14$ Hz, $\omega_Q = 2\pi \times 2.24$ MHz [28], and $T_{2,SC} = 0.090±.014$ s gives a correlation time $\tau = 4.7±0.7$ ps, a similar value to that measured using ^{1}H NMR linewidth analysis [28].

In vivo T_2 measurements of [^{13}C] urea and [^{13}C, ^{15}N$_2$] urea reported in this manuscript differ considerably from those measured in solution. Particularly, the T_2 of [^{13}C, ^{15}N$_2$] urea decreases to less than 2 s in blood, while that of [^{13}C] urea increases from 0.09 s in solution to 0.28 s in blood. This can be at least partially explained by the high blood viscosity due to hematocrit which increases τ. The slowed rotation will affect [^{13}C, ^{15}N$_2$] urea and [^{13}C] urea in the opposite manner [(7) and (6), respectively]. However, there is likely a strong paramagnetic relaxation enhancement due to deoxygenated hemoglobin; this effect has been extensively studied in ^{1}H CPMG experiments. [32]-[34]. Urea is likely to be nearly as prone to this effect as water due to its high permeability through the red blood cell membrane [35], and the intracellular urea pool has been previously observed by ^{13}C NMR via a small (~ 0.2 PPM) frequency shift [36].

III. Methods

A. Sample Preparation

Samples of 6.0 M enriched [^{13}C] urea and [^{13}C, ^{15}N$_2$] urea (Sigma Aldrich, St. Louis, MO, USA) were prepared in a glycerol solution. This mixture was doped with 15 mM of the trityl radical and 1.5 mM Gd-DOTA for polarization enhancement.

B. Hardware

Dynamic nuclear polarization was performed with an Oxford Instruments Hypersense unit (Oxford Instruments, Oxford, U.K.) operating at 1.3 K and 3.35T ($\omega_e = 94.1$ GHz). Imaging and phantom experiments were performed using a custom designed ^{13}C/^{1}H transmit/receive birdcage coil placed in the center of the bore of a 3T ($\omega_C = 32.1$ MHz) clinical imaging system (GE Medical Systems, Waukesha, WI, USA). The scanner gradients had a 4 G · cm^{-1} peak amplitude, 1.5 G · cm^{-1} ms^{-1} peak slew rate.

C. Phantom Measurements

T_1 and T_2 measurements were performed on hyperpolarized [^{13}C] urea and [^{13}C, ^{15}N$_2$] urea in aqueous solution at 37 °C, $B_0 = 3$ T.T_2 measurements were performed with a CPMG sequence with $TR = 2\pi_{CPMG} = 10$ ms, 2000 repetitions, 10 A/D samples per repetition, total duration 20 s. T_1 measurements used an adiabatic double spin echo sequence [37] with a 5° excitation, $TR = 3$ s, 64 scans, 192 s total duration. All experiments were repeated three times. Data were fit to a single exponential decay.

T_2 measurements were performed at various bulk viscosity values which were generated by changing ratios of glycerol/water mixtures to approximate the effect of varying the rotation correlation time τ. The viscosity (in cP) was estimated as a function of glycerol fraction and temperature using the empirical relations given by Cheng [38]. Six 2-mL vials were prepared at differing glycerol concentrations, temperature controlled to 37 °C with a water heat bath, mixed with 20 μL hyperpolarized urea solution, and were imaged with the SSFP sequence with $\theta = 180°$. This sequence played the preparation pulse only once, and during the spin echo train, multiple images were phase encoded

$$\underbrace{\frac{\pi}{2} - \frac{TR}{2}}_{\text{excitation}} - \underbrace{\left(\underbrace{(\pi \times (-1)^n - TR)^n}_{\text{phaseencoding}} \right)^m}_{T_2 \text{ measurement}} .$$

(8)

Parameters used were $n = 32$ phase encodes per image, $TR = 12$ ms, 384 ms per image, $m = 60$ total images over 23 s. In an identical manner, T_2 measurements of [^{13}C] urea and [^{13}C, ^{15}N$_2$] urea in 20%, 40%, and 60% fetal bovine serum were performed.

T_2 measurements were also performed in whole rat blood and plasma. Approximately 2 mL venous blood was drawn from anesthetized rats' lateral tail veins, anticoagulated with K2-EDTA, maintained at 37 °C, injected with hyperpolarized urea solution ($< 5\%$ total volume), gently mixed, and measured via nonselective CPMG acquisitions. The time between blood draw and NMR measurement was kept less than 10 min. This experiment was repeated five times for each urea isotope. For an additional two cases, the whole blood samples were centrifuged at 1000 RCF for 10 min, and the plasma supernatant was gently extracted with a pipette. The T_2 of both urea isotopes were measured in the extracted plasma.

D. Animal Imaging Experiments

Animal studies were performed under a protocol approved by the UCSF Institutional Animal Care and Utilization Committee (IACUC). Experiments used male Sprague Dawley rats (400 ± 100 g) anesthetized with an isoflurane/oxygen mixture. Anatomic T_2-weighted ^{1}H fast spin echo (FSE) images were acquired in the axial and coronal planes. ^{13}C transmitter calibrations were performed by finding the null of the signal response of a vial containing 1 mL of 8M ^{13}C urea solution placed next to the animal. 107 ± 3 mg samples of urea were polarized for 2.5 h (approximately three buildup-time constants) and then dissolved in 5 mL phosphate buffered saline yielding a final solution of approximately 110 mM. [^{13}C] urea samples were transported to the scanner with a bar magnet to avoid signal loss due to low-field T_1 shortening [22]. 3 mL (giving approximately 0.3 millimoles ^{13}C) of the hyperpolarized urea solution were injected into a tail vain catheter over 12 s.

1) T_2 Mapping—$^{13}CT_2$ mapping was performed after infusion of hyperpolarized [^{13}C] urea and [^{13}C, ^{15}N$_2$] urea in four different rats. The imaging was initiated 30 s after the beginning of injection (18 s after end of the injection) to ensure a thorough distribution of the contrast agent through the vasculature and kidneys. Furthermore, the long delay time minimized bolus arrival effects during imaging.

As with the phantom experiments, the preparation (excitation) pulse was played only once, and a refocusing pulse train (using SSFP phase cycling) followed in which *m* dynamic images were acquired (8). Due to the greatly varying T_2 values, the TR and resolution were modified for each isotope. [^{13}C, ^{15}N$_2$] urea: 64×64 encodes over an 8 cm FOV, $TR = 12$ ms giving 0.768 s per image, $m = 20$ images acquired over 15 s. [^{13}C] urea: 20×20 encodes over an 8 cm FOV, $TR = 10$ ms giving 0.200 s per image, $m = 8$ images acquired over 1.6 s.

In pixels in which the first time point SNR was greater than 30, the time-decay curves after injection of [^{13}C, ^{15}N$_2$] urea were fit to the bi-exponential model

$$S\left(t,x,y\right) = A_S\left(x,y\right)e^{-t/T_{2,S}\left(x,y\right)} + A_L\left(x,y\right)e^{-t/T_{2,L}\left(x,y\right)}. \quad (9)$$

$T_{2,S}$, the short T_2 component, was constrained to [0,2] s, and the long component T_2 was constrained to [2, 100] s. Fitting was performed in MATLAB using the trust region algorithm (with the function lsqcurvefit). Single labeled [^{13}C] urea was fit to a single exponential decay

$$S\left(t,x,y\right) = A\left(x,y\right)e^{-t/T_2(x,y)} \quad (10)$$

due to the difficulty in bi-exponential fitting with a limited number of data points. As before, fitting was only performed in regions with first time point SNR > 30. After fitting, only pixels with $R^2 > 0.95$ were included in analysis. T_2 values from pixels within the aorta, renal cortex and medulla, and renal pelvis (selected using manually-drawn margins) were fit to a normal distribution to estimate mean and variance. The long T_2 component ($T_{2,L}$) distributions were highly asymmetric and were fit to a type II generalized extreme value (Frechet) distribution

$$PDF\left(x\right) = \frac{1}{s}g(x)^{-1-1/k}exp\left[-g(x)^{-1/k}\right] \quad (11)$$

$$g\left(x\right) = 1 + k\frac{\left(x-\mu\right)}{s} \quad (12)$$

where μ is the location parameter μ, is the scale parameter, and *k* shape parameter. This distribution was chosen since it captures the finite lower limit imposed by constrained bi-exponential fitting, the asymmetry of the distribution, and the long observed tails at high $T_{2,L}$ values. After estimation of *s*, *k*, and μ, the means and standard deviations were calculated as $\mu - s/k + (s/k)g_1$ and $(s/k)\sqrt{g_2 - g_1^2}$, respectively, with $g_n = \Gamma(1 - nk)$ and $\Gamma\left(z\right) = \int_0^\infty t^{z-1}e^{-tz}dt$

2) SSFP Imaging SNR Comparison—To measure the improvement in image quality associated with the longer T_2 of [^{13}C, ^{15}N$_2$] urea, repeat *in vivo* hyperpolarized imaging experiments with [^{13}C] urea and [^{13}C, ^{15}N$_2$] urea were performed back-to-back in six different animals. All imaging was initiated 20 s after the start of the injection. Similar to previous implementations [13], the acquisition was aligned in the coronal plane with no slice-select gradients (projection mode) and phase encoding set along the right/left dimension to avoid image aliasing. 96×96 ($n = 4$) and 192×96 ($n = 2$) images were acquired with, $TR = 15$ ms, $TE = 7.5$ ms, 4.8 ms data acquisition time per TR. All acquisition had a 208 Hz/pixel receive bandwidth. Since this value is much greater than the 19 Hz J-coupling constant of [^{13}C, ^{15}N$_2$] urea, no imaging SNR loss was expected from the spectral splitting. [^{13}C, ^{15}N$_2$] urea acquisitions used $\theta = 180°$, and [^{13}C] urea acquisitions used $\theta = 35°$. These values were picked to maximize the signal using the aqueous solution T_2 values, and as we will show, the latter value was slightly suboptimal for *in vivo* T_2 values. One experiment in which [^{13}C] urea was imaged with $\theta = 35°$, 50°, 70° and 180° was performed to highlight the need for lower θ values with the short T_2 urea. All experiments used a 3.2 ms time-bandwidth product = 4 windowed sinc pulse which gives a $\theta = 180°$ rotation on resonance at 0.6 G.

IV. Results

A. Phantom Measurements

Table I gives aqueous solution T_1, T_2, and polarization measurements. The T_2 values of [^{13}C] urea and [^{13}C, ^{15}N$_2$] urea differed substantially in solution, with the differences being highest in dilute aqueous solutions. Both compounds showed similar T_1 values. The polarization of [^{13}C] urea was slightly lower and showed more variability from run to run. Even though the sample was transported with a bar magnet, there was likely some residual scalar coupling T_1 relaxation during transport. Fig. 4 shows the measured T_2 in whole blood, serum, plasma, and water. The blood and plasma values are also listed in Table I. Fetal bovine serum caused some relaxation enhancement of [^{13}C, ^{15}N$_2$] urea, which is likely due to reduced τ or some degree of protein binding. The [^{13}C, ^{15}N$_2$] urea T_2 was greatly reduced between plasma and whole blood indicating a strong relaxivity from red blood cells.

Fig. 3 shows the T_2 behavior of both urea isotopes with modulation of the correlation time via changing the bulk solution viscosity. The scalar coupling pathway clearly dominates the [^{13}C] urea T_2. Since the rotational correlation time and viscosity are linearly related for approximately spherical molecules from the Debye–Hückel relation, from (4), (6), and (7) the T_2 of [^{13}C, ^{15}N$_2$] urea should scale approximately as η^{-1} and that of [^{13}C] urea should scale as η^{+1}. The actual powers measured from fitting the data in Fig. 3 were -0.73 ± 0.20 and 0.87 ± 0.05, respectively. Some deviation of the expected powers of -1 and 1 is expected due to the well known discrepancies between macroscopic and microscopic in solution viscosities [39]. Furthermore, [^{13}C] urea will have some weak contribution from dipolar and CSA which will scale as η^{-1}.

B. In Vivo Experiments

1) T_2 Mapping—Results from T_2 mapping experiments are shown in Fig. 5. The [^{13}C, ^{15}N$_2$] urea experiments showed a largely short scale ~ 1.3 s $T_{2,S}$ decay throughout the animal which is presumed to be the vascular urea component. Bi-exponential fitting showed the long $T_{2,L}$ component almost completely isolated to the kidneys. The large mean values of these components are given in Table II. While these values are potentially contaminated by collection of the agent into the inner regions of the kidney during the imaging time, the longer T_2 are believable since signal likely represents that from the glomerular filtrate. Since the filtrate is free from red blood cells and plasma proteins some recovery of the solution T_2 can be expected. The filtered urea in the medulla and cortex is primarily in the tubules and medullary interstitium, so some restriction of motion will likely cause a reduced τ and T_2 shortening compared to that dilute solution. However, in the renal pelvis, the large liquid pool will give a reduced τ and virtually all the solution T_2 is recovered. The short T_2 component observed in the kidney likely arises from blood above and below the kidney (due to the projection imaging mode) and possibly also from the renal vasculature. Some long T_2 component was observed in the inferior aorta and femoral branches. This is likely due to RF transmitter drop-off causing some T_1 contamination to the decay curve. However, slower flow could also be a factor.

Due to the much shorter T_2 of [^{13}C] urea, the T_2 mapping images had to be acquired with a much coarser resolution. With the limited number of time samples available, bi-exponential fitting was not possible. However, a slightly shorter mean T_2 within the kidney compared to that measured in the aorta was be observed. This is concordant with solution measurements that show that [^{13}C] urea and [^{13}C, ^{15}N$_2$] urea respond to differences in τ in the opposite manner.

Table II summarizes the histogram fitting of the T_2 mapping experiments. The distributions of [^{13}C, ^{15}N$_2$] urea $T_{2,S}$ were approximately normal within the kidney, and the $T_{2,S}$ measured from the medulla and renal pelvis had very similar mean values. $T_{2,S}$ values within the aorta were slightly higher. This is potentially due to the fact that the aorta is fed superiorly from the heart, which in these experiments was at the edge of the transmitter. $T_{2,L}$ distributions within the kidney were highly asymmetric and were fit to a Frechet distribution. $T_{2,L}$ values had a similar shape parameter k in the medulla and pelvis. Since there was no though-slice localization, it is not possible to determine whether the asymmetry of the distributions represents some geometry factor (stemming from summing all the pixels through the kidney in one dimension), medulla/pelvis partial voluming, or an actual distribution reporting on a physiological parameter. In all likelihood, the decays show more than two characteristic decay times. The reported mean $T_{2,L}$ in the pelvis of 11.0±1.8 s is likely an underestimate since $T_{2,L}$ the parameter also incorporated the faster relaxing medulla immediately above and below the pelvis. Determination of all the characteristic decay times is very difficult, however, due to the ill-conditioned nature of multi-exponential fitting.

2) SSFP Imaging Comparisons—In one rat, hyperpolarized [^{13}C] urea was imaged with varying τ values. These images are shown in Fig. 7 along with the SNR values

measured in the aorta and kidney. With the lower τ necessary for imaging the short T_2 urea at high resolution, the images were susceptible to signal drop-off from banding artifacts. At flip angles sufficiently high to alleviate the banding, the overall signal is greatly decreased due to T_2. The SNR curve resembles its simulated counterpart in Fig. 1, top left, indicating an SNR-optimal τ around 50°. Although the $\tau = 35°$ used for imaging comparisons was slightly suboptimal, only an additional 20%–30% signal increase can be expected with use of a higher flip. Furthermore, as indicated in Fig. 1, bottom left, blurring effects will become very problematic in this regime. The image SNR was too low to detect significant blurring, however. A potential solution for yielding favorable signal behavior when the imaging time is much greater than T_2 is the use of progressive flip angle SSFP acquisitions. [40]. This method would require a good estimate of T_2 for flip angle calculations which may introduce difficulty when multiple, greatly varying T_2 values are present.

Fig. 6 shows high resolution imaging comparisons of [^{13}C] urea and [^{13}C, ^{15}N$_2$] urea for two different comparisons. Resolution was sufficient to discern the aorta, renal, common and external iliac, medial sacral, and femoral arteries in all [^{13}C, ^{15}N$_2$] urea images. The kidneys showed a mean SNR of 260 ± 100. [^{13}C] urea images had lower SNR expected from the use of lower flip angles; however, in many cases, the SNR difference between [^{13}C] urea and [^{13}C, ^{15}N$_2$] urea images differed substantially more than the factor of ~ 3 expected from simulations (Fig. 1). There was evidence of banding artifact with the use of lower flip angles; this was significant in the image shown Fig. 6, bottom right. In the upper right image in Fig. 6, this artifact is less detrimental but is still present in the region near the iliac branch.

Some differences in contrast are noted in the SSFP images acquired at different flip angles which is expected based on the differing T_2 weighing. SSFP images acquired with lower flip angles tended to have more diffuse background signal; this can be seen in Fig. 6 comparing the bottom two images. The source of this background is unclear, but may it may represent capillary signal with short T_2.

Fig. 8 shows the mean and standard deviation of SNR values measured in the aorta and kidneys of each imaging comparison. Since the dose was not normalized to the animal mass, there is significant subject-to-subject SNR variability. The lower plots in Fig. 8 show the ratio of the SNR values measured in each subject which should normalize to the dose variations. Large variations are observed even in the SNR ratios which is inevitable due to some differences in sample transport time, run-to-run polarization levels, and residual scalar coupling relaxation which diminishes [^{13}C] urea polarization. However, all [^{13}C, ^{15}N$_2$] urea showed at least a doubling in SNR, with a mean increase of 4.9±0.6 in the kidneys and 4.7±1.0 in the aorta.

V. Discussion

The high sensitivity of hyperpolarization is offset by the low intrinsic sensitivity of the ^{13}C nucleus, requiring large doses. Therefore, some estimate of the safety of this dose level is warranted to estimate its potential clinical translatability. As mentioned in the introduction, steady state blood urea concentrations of 5.5±2.0 mM(33 ± 12 mg/dL) are typical in healthy

humans and rats. For experiments conducted in this study, the estimated blood urea concentration after bolus injection was 12±3 mM(71 ± 20 mg/dL) which was calculated from the 400±100 g mass of the animals used in the study and their estimated blood volumes of 25 ± 6 mL [41]. This value is approximately double the steady state blood urea concentration. The worst-case anticipated safe dose can be inferred from a study by Johnson *et al.* [21] in which patients with advanced stage renal failure were loaded with urea (added to the dialysate) to maintain steady state blood urea concentrations of 181–600 mg/dL for periods of 7–90 days. Doses of less than 300 mg/dL were well tolerated, while doses from 300–600 mg/dL were associated with malaise, vomiting, and headache [20], [42]. Based on these results, we expect doses at least four times higher than those used in this imaging study to be well tolerated in patients with advanced renal failure. This figure is almost certainly an underestimate since the patients from the Johnson *et al.* study were maintained at high urea doses for multiple days. Subjects with normal kidney function will also certainly tolerate much larger doses.

In order to extract the large SNR increases from increased T_2, long trains of refocusing pulses were used. The SAR of this sequence compared to that used for ^{1}H imaging can be roughly estimated by assuming a uniform sphere with diameter long compared to the wavelength ($\lambda = 9.3$ m for ^{13}C at 3T). Using this model, the power dissipated in the sphere scales as $\omega_0^2 B_1^2$ [43]. Compared to ^{1}H, ω_0 is reduced by a factor of γ_c/γ_h, the ratio of the gyromagnetic ratios, and the peak B_1 is increased by the same factor for a given flip angle. Therefore, the ^{13}C spin echo trains have similar SAR as the ^{1}H sequence with identical pulse widths, pulse time-bandwidth products, and timing parameters. The large TR values necessary for the larger imaging gradient lobes imply that the SAR is actually lower than that of a typical CPMG imaging sequence for ^{1}H.

Although all imaging in this manuscript was performed in projection mode so that slice profile effects would not contaminate T_2 and SNR measurements, extension to multi slice or 3D imaging should be straight forward. Multi slice imaging was performed in several previous hyperpolarized SSFP implementations [15]–[17], [24]. For isotropic resolution, 3D imaging should also be possible, but due to the larger number of phase encoding steps, a flip angle less than 180° will likely be required. All T_2 values measured in this manuscript must be considered effective T_2 values due to the numerous factors confounding measurements. Given the SSFP signal response given by (1), RF transmitter variations will deviate θ from 180° thus adding some T_1 weighting to the signal decay. Over a series of spin echo pulses, the net transverse relaxation rate can differ significantly from the true R_2. The diffusion attenuation can be expressed as

$$\tilde{R}_2 = R_2 + \frac{b(t)D}{TR} + \frac{1}{12}D\gamma^2\bar{G}^2 TR^2 \quad (13)$$

where R_2 is the true rate, $\tilde{R}_2$ the observed rate, $b(t) = (2\pi)^2 \int_0^t |\vec{k}(t')|^2 \, dt'$ with $\vec{k}(t) = \gamma/2\pi \int_0^t G(t') \, dt'$ is the diffusion weighting due to imaging gradients [24], and the term $(1/12)D\gamma^2\bar{G}^2 TR^2$ represents the diffusion through local B_0 variations (modeled as a

constant gradient $\bar{G}$) [44]. Although the diffusion term on the left restricts the flip angle choice for hyperpolarized noble gases [24] due to D values in the range of 0.1–2 cm^2/s [45], the diffusivity of ^{13}C labeled small molecules in solution is between three and five orders of magnitude lower. While this makes liquid state ^{13}C diffusion weighted imaging more difficult on a clinical scanner due to the difficulty in achieving large signal attenuation, this is a favorable characteristic for multiple spin echo imaging since the diffusion weighing will not widen the point spread significantly. The apparent diffusion coefficient for urea was measured to be 1.54×10^{-3} mm^2/s at 27°C [46]. Given the total b value $b(N_{PE}TR = 6.5$ s/mm^2 integrated over all frequency and phase encoding pulses over 96 repetitions, the diffusion weighting is exp $[b(N_{PE}TR)D] \approx 0.99$. Although the imaging gradient weighting is likely negligible, the microscopic diffusion term likely contaminates T_2 measurements to some degree due to the relatively long (10–15 ms) TR values used and the potentially large gradient $\bar{G}$ experienced by the urea molecule in its transport in and out of the red blood cell. This effect is difficult to quantify *in vivo*; previous studies isolating this effect used T_2 dispersions experiments which measure the dependency of T_2 on $TR = 2\pi_{CPMG}$[32]–[34].

Bulk flow parallel to the imaging gradients will induce some phase, and if this phase not coherent within a voxel, this will lead to some signal loss. The frequency encoding gradients in SSFP sequences are first-moment flow compensated, so constant-velocity flow along the frequency encoded direction is fully rephased. The phase encode gradients had a peak first moment $\int_0^{TR} G(\tau)\tau, d\tau$ of 0.039 s/cm, leading to a ~ 2° phase shift for a 1 cm/s velocity. Although this value is quoted for the outer k space lines, some destructive interference from phase-induced flow over 96 phase encodes (acquired over 1.4 s) could lead to signal loss. This is very likely the source of the large discrepancy of T_2 values measured in whole blood (Table I) and *in vivo* (Table II). In addition to the potential signal attenuation due to flow and diffusion effect, there is likely some lengthening of the measured T_2 in the inner regions of the kidney due to collection during the imaging time.

The extremely long T_2 values measured within the kidney is in itself a potential source of interesting imaging contrast. In this study we were not able to definitively attribute the long T_2 component to urea within the filtration and collecting system. However, this seems very likely given the anatomical distributions of the long T_2 component. Relaxation time gradients between the cortex, medulla, and pelvis are well known from ^{1}H experiments [47], but the direct measurement of urea within the blood and filtered pools could be a powerful tool for assessment of the urea concentrating function of the kidney.

VI. Conclusion

This study demonstrated a greatly increased imaging SNR of hyperpolarized ^{13}C urea associated with ^{15}N labeling of the amide nitrogens. The SNR increase was due to a very large T_2 increase associated with the elimination of a strong scalar coupling relaxation pathway, and this allowed for SSFP acquisitions with flip angles in the fully refocused regime on a clinical scanner with large minimum TR constraints. Projection images were acquired with in-plane resolution of 1 mm with SNR of 230 ± 120 in the aorta and $260 \pm$

100 in the kidney. *In vivo* T_2 mapping showed spatially heterogeneous T_2 values, with values of 1.3 s typical in the blood and greater than 10 s observed in the kidney.

Acknowledgments

References

[1]. Kurhanewicz J, Vigneron DB, Brindle K, Chekmenev EY, Comment A, Cunningham CH, Deberardinis RJ, Green GG, Leach MO, Rajan SS, Rizi RR, Ross BD, Warren WS, Malloy CR. Analysis of cancer metabolism by imaging hyperpolarized nuclei: prospects for translation to clinical research. Neoplasia. Feb; 2011 13(2):81–97. [PubMed: 21403835]

[2]. Ardenkjaer-Larsen JH, Fridlund B, Gram A, Hansson G, Hansson L, Lerche MH, Servin R, Thaning M, Golman K. Increase in signal-to-noise ratio of > 10,000 times in liquid-state NMR. Proc. Nat. Acad. Sci. USA. Sep; 2003 100(18):10158–63. [PubMed: 12930897]

[3]. Johannesson H, Macholl S, Ardenkjaer-Larsen JH. Dynamic nuclear polarization of [1–^{13}C] pyruvic acid at 4.6 tesla. J. Magn. Reson. 2009; 197(2):167–175. [PubMed: 19162518]

[4]. Golman K, Zandt R, Thaning M. Real-time metabolic imaging. Proc. Nat. Acad. Sci. USA. 2006; 103(30):11270–11275. [PubMed: 16837573]

[5]. Gallagher FA, Kettunen MI, Hu D-E, Jensen PR, Zandt RI, Karlsson M, Gisselsson A, Nelson SK, Witney TH, Bohndiek SE, Hansson G, Peitersen T, Lerche MH, Brindle KM, Shan L. Hyperpolarized [1,4–^{13}C$_2$]fumarate as an imaging agent of tumor cell death in vivo. Proc. Nat. Acad. Sci. USA. Nov; 2009 106(47):19801–6. [PubMed: 19903889]

[6]. Gallagher FA, Kettunen MI, Brindle KM. Imaging pH with hyperpolarized ^{13}C. NMR Biomed. 2011; 24(8):1006–1015. [PubMed: 21812047]

[7]. Keshari KR, Kurhanewicz J, Bok R, Larson PEZ, Vigneron DB, Wilson DM. Hyperpolarized ^{13}C dehydroascorbate as an endogenous redox sensor for in vivo metabolic imaging. Proc. Nat. Acad. Sci. USA. 2011; 108(46):18606–18611. [PubMed: 22042839]

[8]. Golman K, Zandt R, Lerche M, Pehrson R, Ardenkjaer-Larsen JH. Metabolic imaging by hyperpolarized ^{13}C magnetic resonance imaging for in vivo tumor diagnosis. Cancer Res. 2006; 66(22):10855–10860. [PubMed: 17108122]

[9]. Brindle KM, Bohndiek SE, Gallagher FA, Kettunen MI. Tumor imaging using hyperpolarized ^{13}C magnetic resonance spectroscopy. Magn. Reson. Med. 2011; 66(2):505–519. [PubMed: 21661043]

[10]. Keshari KR, Sriram R, Koelsch BL, Criekinge MV, Wilson DM, Kurhanewicz J, Wang ZJ. Hyperpolarized ^{13}C-pyruvate magnetic resonance reveals rapid lactate export in metastatic renal cell carcinomas. Cancer Res. 2013; 73(2):529–538. [PubMed: 23204238]

[11]. Bohndiek SE, Kettunen MI, Hu D-E, Kennedy BWC, Boren J, Gallagher FA, Brindle KM. Hyperpolarized [1–^{13}C]-ascorbic and dehydroascorbic acid: Vitamin C as a probe for imaging redox status in vivo. J. Am. Chem. Soc. Aug; 2011 133(30):11795–801. [PubMed: 21692446]

[12]. Golman K, Ardenkjaer-Larsen JH, Petersson JS, Mansson S, Leunbach I. Molecular imaging with endogenous substances. Proc. Nat. Acad. Sci. USA. 2003; 100(18):10435–10439. [PubMed: 12930896]

[13]. Svensson J, Mansson S, Johansson E, Petersson JS, Olsson LE. Hyperpolarized C-13 MR angiography using truefisp. Magn. Reson. Med. 2003; 50(2):256–262. [PubMed: 12876701]

[14]. Johansson E, Mansson S, Wirestam R, Svensson J, Petersson J, Golman K, Stahlberg F. Cerebral perfusion assessment by bolus tracking using hyperpolarized ^{13}C. Magn. Reson. Med. 2004; 51(3):464–472. [PubMed: 15004786]

[15]. Olsson LE, Chai C-M, Axelsson O, Karlsson M, Golman K, Petersson JS. MR coronary angiography in pigs with intraarterial injections of a hyperpolarized ^{13}C substance. Magn. Reson. Med. 2006; 55(4):731–737. [PubMed: 16538605]

[16]. Johansson E, Olsson LE, Mansson S, Petersson J, Golman K, Stahlberg F, Wirestam R. Perfusion assessment with bolus differentiation: A technique applicable to hyperpolarized tracers. Magn. Reson. Med. 2004; 52(5):1043–1051. [PubMed: 15508152]

[17]. Morze, C. v.; Larson, PEZ.; Hu, S.; Keshari, K.; Wilson, DM.; Ardenkjaer-Larsen, JH.; Goga, A.; Bok, R.; Kurhanewicz, J.; Vigneron, DB. Imaging of blood flow using hyperpolarized [^{13}C] urea in preclinical cancer models. J. Magn. Reson. Imag. Mar; 2011 33(3):692–7.

[18]. Grant AK, Vinogradov E, Wang X, Lenkinski RE, Alsop DC. Perfusion imaging with a freely diffusible hyperpolarized contrast agent. Magn. Reson. Med. 2011; 66(3):746–755. [PubMed: 21432901]

[19]. Gardner MD, Scott R. Age- and sex-related reference ranges for eight plasma constituents derived from randomly selected adults in a Scottish new town. J. Clin. Pathol. 1980; 33:380–385. [PubMed: 7400337]

[20]. Anderson AK, Honeywell HE, Santy AC, Pedersen S. The composition of normal rat blood. J. Biol. Chem. 1930; 86(1):157–160.

[21]. Johnson W, Hagge W, Wagoner R, Dinapoli R, Rosevear J. Effects of urea loading in patients with far-advanced renal failure. Mayo Clin. Proc. 1972; 47(1):21–29. [PubMed: 5008253]

[22]. Chiavazza E, Kubala E, Gringeri CV, Duwel S, Durst M, Schulte RF, Menzel MI. Earth's magnetic field enabled scalar coupling relaxation of nuclei bound to fast-relaxing quadrupolar in amide groups. J. Magn. Reson. 2013; 227(0):35–38. [PubMed: 23262330]

[23]. Yen Y-F, Roux PL, Mayer D, King R, Spielman D, Tropp J, Pauly KB, Pfefferbaum A, Vasanawala S, Hurd R. T_2 relaxation times of ^{13}C metabolites in a rat hepatocellular carcinoma model measured in vivo using ^{13}C-MRS of hyperpolarized [1–^{13}C] pyruvate. NMR Biomed. 2010; 23(4):414–423. [PubMed: 20175135]

[24]. Wild JM, Teh K, Woodhouse N, Paley MN, Fichele S, Zanche N. d. Kasuboski L. Steady-state free precession with hyperpolarized ^{3}He: Experiments and theory. J. Magn. Reson. 2006; 183(1): 13–24. [PubMed: 16890464]

[25]. Leupold J, Månsson S, Petersson JS, Hennig J, Wieben O. Fast multiecho balanced SSFP metabolite mapping of ^{1}H and hyperpolarized ^{13}C compounds. MAGMA. Aug; 2009 22(4):251–6. [PubMed: 19367422]

[26]. Bhattacharya P, Harris K, Lin A, Mansson M, Norton V, Perman W, Weitekamp D, Ross B. Ultra-fast three dimensional imaging of hyperpolarized in vivo. MAGMA. 2005; 18:245–256. [PubMed: 16320090]

[27]. Scheffler K. On the transient phase of balanced SSFP sequences. Magn Reson Med. 2003; 270:781–783. [PubMed: 12652552]

[28]. Finer EG, Franks F, Tait MJ. Nuclear magnetic resonance studies of aqueous urea solutions. J. Am. Chem. Soc. 1972; 94(13):4424–4429.

[29]. Abragam, A. Principles of Nuclear Magnetism. Oxford Univ. Press; New York: 1983.

[30]. Sharp RR, Tolan JW. Nuclear magnetic relaxation of ^{119}Sn, ^{35}Cl, and ^{127}I in two symmetric top molecules, SnCl$_3$ and SnI$_3$Cl, in liquid mixtures. J. Chem. Phys. 1976; 65(2):522–530.

[31]. Gryff-Keller A, Kubica D. Scalar relaxation of the second kind: A potential source of information on the dynamics of molecular movements. 1. investigation of solution reorientation of *N*-methylpyridone and 1,3-dimethyluracil using measurements of longitudinal relaxation rates in the rotating frame. J. Phys. Chem. A. 2012; 116(39):9632–9638. [PubMed: 22971246]

[32]. Thulborn KR, Waterton JC, Matthews PM, Radda GK. Oxygenation dependence of the transverse relaxation time of water protons in whole blood at high field. Biochim. Biophys. Acta. 1982:265–270. [PubMed: 6275909]

[33]. Gomori JM, Grossman RI, Yu-Ip C, Asakura T. NMR relaxation times in blood: Dependence on field strength, oxidation state, and cell integrity. J. Comput. Assist. Tomogr. 1987; 11(4):684–690. [PubMed: 3597895]

[34]. Meyer M-E, Yu O, Eclancher B, Grucker D, Chambron J. NMR relaxation rates and blood oxygenation level. Magn. Reson. Med. 1995; 34:234–241. [PubMed: 7476083]

[35]. Braham J. Urea permeability of human red cells. J. Gen. Physiol. 1983; 82:1–23. [PubMed: 6411854]

[36]. Potts JR, Bulliman BT, Kuchel PW. Urea exchange across the human erythrocyte membrane measured using ^{13}C NMR lineshape analysis. Eur. Biophys. J. 1992; 21:207–216. [PubMed: 1425476]

[37]. Cunningham CH, Chen AP, Albers MJ, Kurhanewicz J, Yen Y-F, Hurd RE, Pauly JM, Nelson SJ, Vigneron DB. Double spin-echo sequence for rapid spectroscopic imaging of hyperpolarized ^{13}C. J. Magn. Reson. 2007; 187(2):357–362. [PubMed: 17562376]

[38]. Cheng N-S. Formula for the viscosity of a glycerol-water mixture. Ind. Eng. Chem. Res. 2008; 47(9):3285–3288.

[39]. Bloembergen N, Purcell EM, Pound RV. Relaxation effects in nuclear magnetic resonance absorption. Phys. Rev. 1948; 73(7):679–712.

[40]. Deppe MH, Wild JM. Variable flip angle schedules in bSSFP imaging of hyperpolarized noble gases. Magn. Reson. Med. 2012; 67(6):1656–1664. [PubMed: 22134846]

[41]. Lee HB, Blaufox MD. Blood volume in the rat. J. Nucl. Med. 1985; 26(1):72–76. [PubMed: 3965655]

[42]. Final report of the safety assessment of urea. Int. J. Toxicol. 2005; 24(3):1–56.

[43]. Collins CM, Wang Z. Calculation of radiofrequency electromagnetic fields and their effects in MRI of human subjects. Magn. Reson. Med. 2011; 65(5):1470–1482. [PubMed: 21381106]

[44]. Carr HY, Purcell EM. Effects of diffusion on free precession in nuclear magnetic resonance experiments. Phys. Rev. 1954; 94:630–638.

[45]. Mugler JP, Altes TA. Hyperpolarized ^{129}Xe MRI of the human lung. J. Magn. Reson. Imag. 2013; 37(2):313–331.

[46]. Koelsch BL, Keshari KR, Peeters TH, Larson PEZ, Wilson DM, Kurhanewicz J. Diffusion MR of hyperpolarized ^{13}C molecules in solution. Analyst. 2013; 138:1011–1014. [PubMed: 23304699]

[47]. Kundel HL, Schlakman B, Joseph PM, Fishman JE, Summers R. Water content and NMR relaxation time gradients in the rabbit kidney. Invest. Radiol. 1986; 21(1):12–17. [PubMed: 3943954]
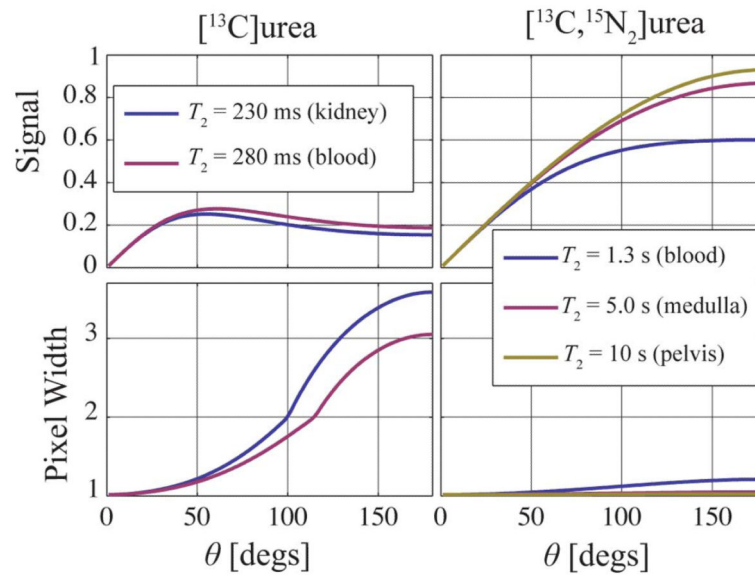
Fig. 1.
Simulated SSFP signal response and pixel width for 96 phase encodes and $TR = 15$ ms, the values used in projection imaging experiments. The data are plotted as a function of SSFP flip angle for both urea isotopes using the estimated T_2 values.
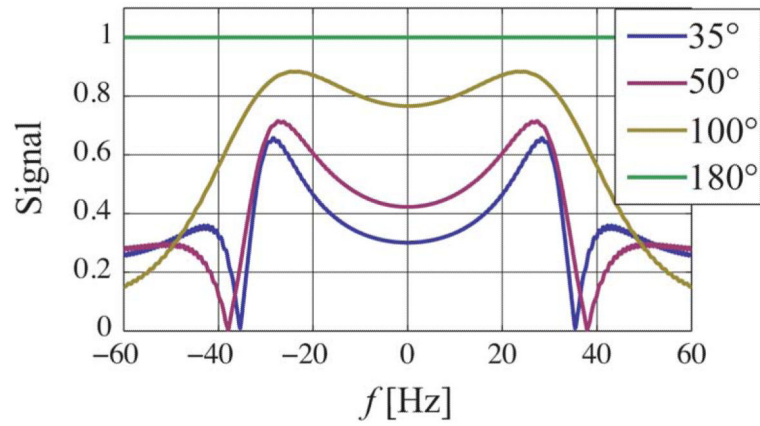
Fig. 2.
Simulated SSFP signal as a function of frequency excluding relaxation and RF selectivity. Due to the small frequency range simulated, RF spectral profile effects were ignored. The signal loss occurring at $\pm 1/2TR$ can be detrimental due to the longer TR required on clinical imaging systems. When T_2 is long compared to the imaging time, the banding can be eliminated with use of larger flip angles.
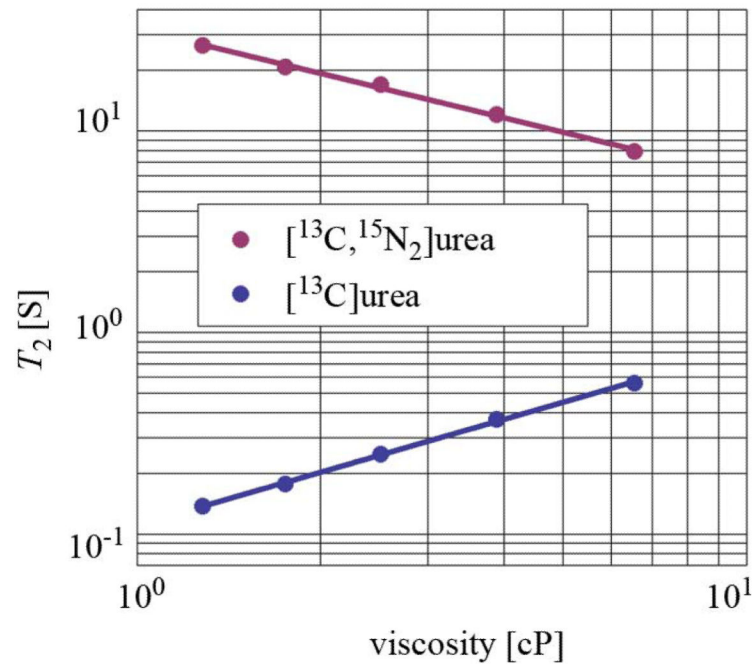
Fig. 3.
Hyperpolarized urea T_2 values as a function of macroscopic viscosity. The removal of the scalar relaxation pathway via ^{15}N labeling gives 13C, [15]N$_2$] urea a much larger T_2 as well as a differing T_2 dependence on correlation time (which should be approximately linear with viscosity).
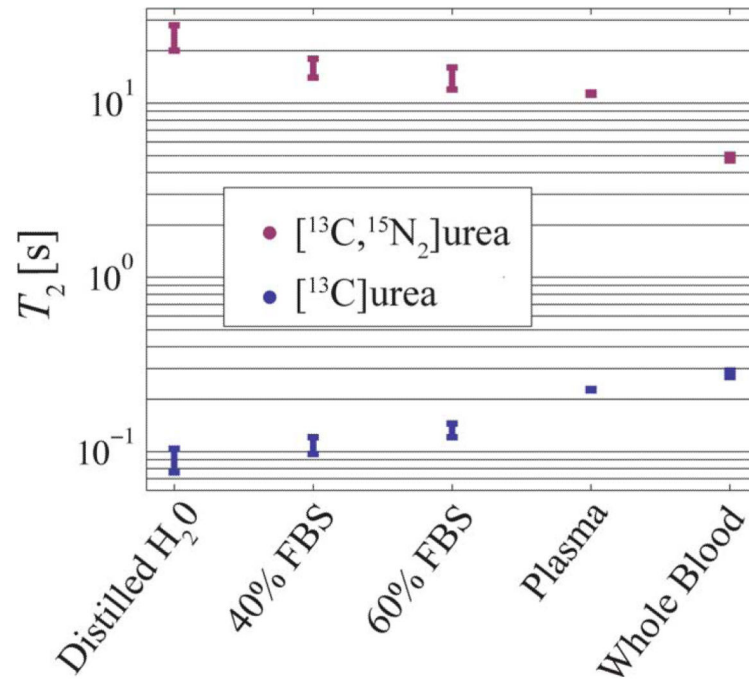
Fig. 4.
Hyperpolarized urea T_2 values in whole blood, serum, plasma, and water. The [^{13}C, ^{15}N$_2$] urea T_2 is greaty reduced in whole blood compared to plasma indicating a strong relaxivity effect from red blood cells.
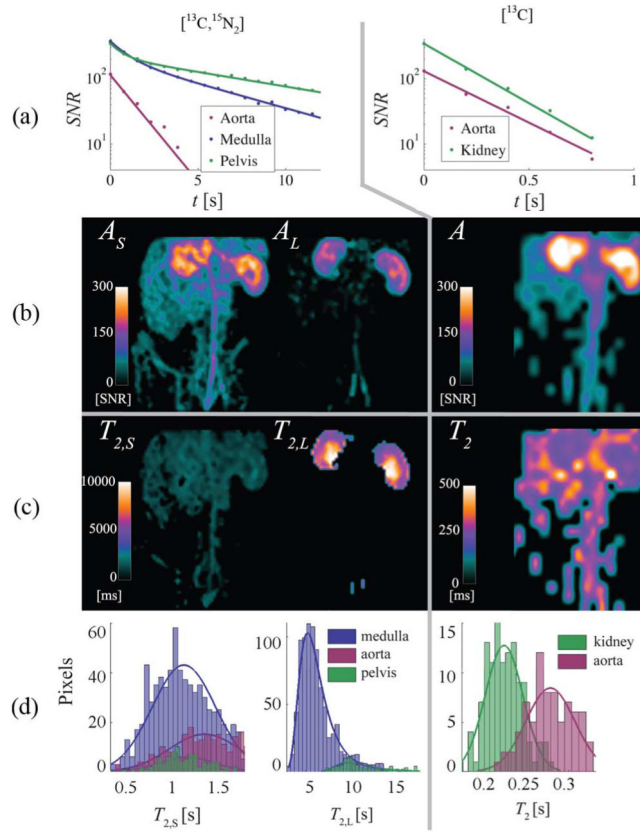
Fig. 5.

(a) Single pixel T_2 decay curves each both urea isotopes measured in the aorta, medulla, and renal pelvis. The $[^{13}C, ^{15}N_2]$ urea decay shows a bilinear slope, and the fast decay rate is similar to that measured in the aorta. This is likely due to the blood above and below the kidney. Signal within the blood fit well to single exponential decays. (b) Fitted amplitudes given by (9) and (10). The long T_2 amplitude A_L is almost completely localized to the kidneys. (c) T_2 maps (in ms). The $[^{13}C, ^{15}N_2]$ urea experiments showed extremely long T_2 components in the kidney, with the greatest values measured in the renal pelvis. The $T_{2,L}$ map was thresholded using the A_L values. The cortex and medulla showed similar values. $[^{13}C]$ urea showed slightly lower T_2 values in the kidneys. (d) histograms showing T_2 distributions of all pixels within the medulla, aorta, and renal pelvis for all four rats. $T_{2,L}$ values approaching the pure solution T_2 of 20 s were detected in some pixels in the renal pelvis.
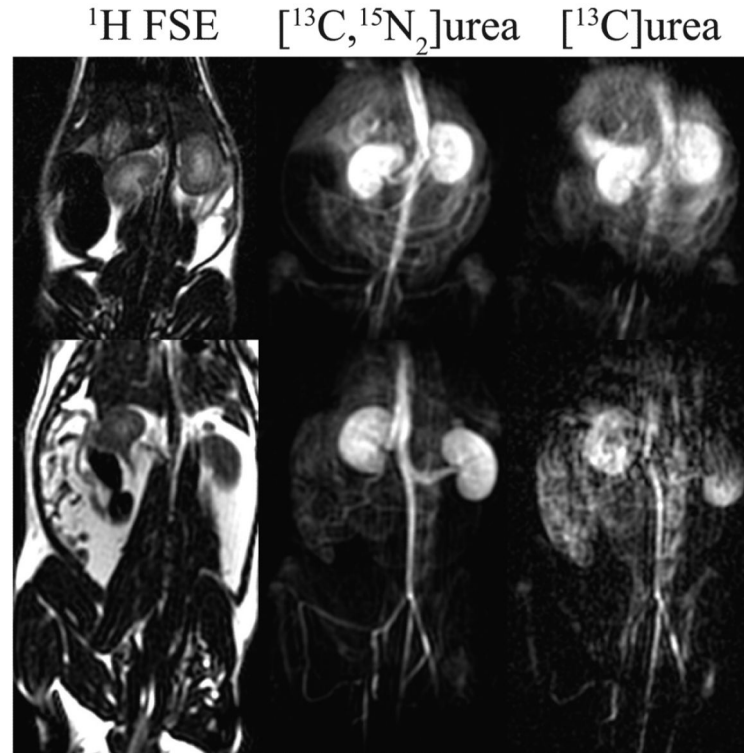
Fig. 6.
Projection imaging at 0.94 mm in-plane resolution. Top: localizer, [^{13}C] urea, and [^{13}C, ^{15}N$_2$] urea images acquired with a 9 cm FOV. Higher SNR and reduced blurring is observed in the [^{13}C, ^{15}N$_2$] urea image. The [^{13}C] urea shows some signal loss due to banding artifact towards the iliac branch. Bottom: [^{13}C] urea and [^{13}C, ^{15}N$_2$] urea images acquired over a 9 × 18 cm FOV. The kidneys were slightly anterior and posterior of the localizer slice. The [^{13}C] urea shows much lower SNR also likely due to banding. The [^{13}C, ^{15}N$_2$] urea image clearly depicts the aorta and its inferior branches. Virtually all [^{13}C, ^{15}N$_2$] urea images showed signal through the femoral arteries with some enhancement in the knee. Spinal vasculature is also depicted in the bottom center image.
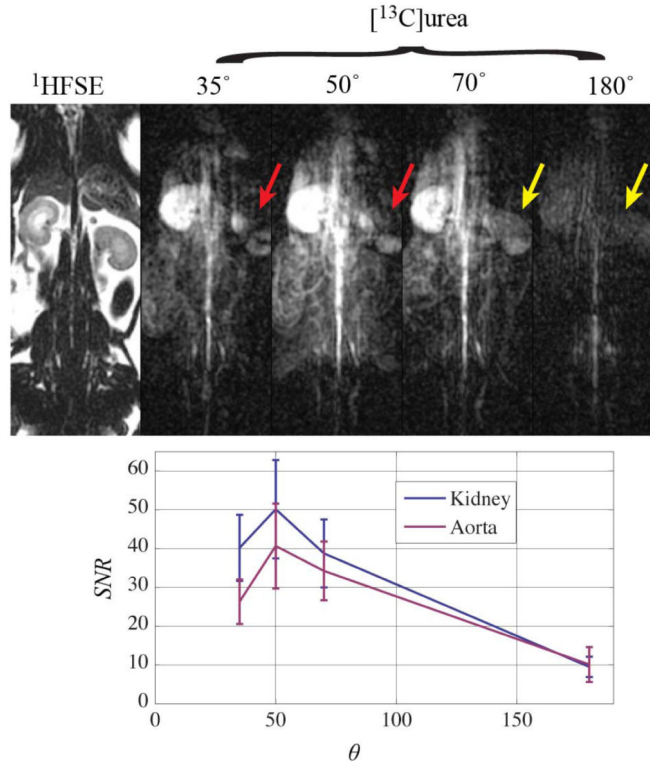
Fig. 7.
Hyperpolarized [^{13}C] urea imaged using an SSFP sequence with multiple θ values (top) highlighting the difficulty in using high flips for the short T_2 urea. Mean SNR values (bottom) are shown with error bars representing standard deviation for the given organ. Only the right kidney SNR values were used due to the banding artifacts (red arrow) in the left kidney. At flip angles sufficiently high to elmininate the banding (yellow arrows), the overall SNR is greatly reduced from a stronger T_2 weighting. The shape of the curves are similar to their simulated counterparts in Fig. 1, top left.
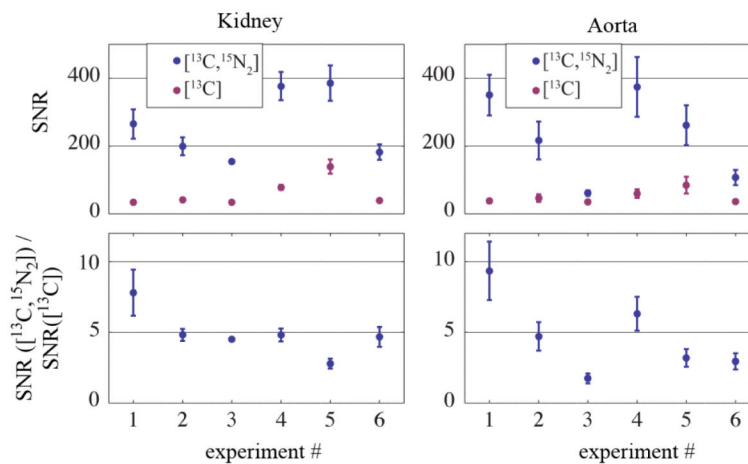
Fig. 8.
Mean SNR values in the kidney and aorta for each SSFP imaging experiment with error bars representing the standard deviations. The SNR ratios [^{13}C, ^{15}N$_2$] urea to [^{13}C] urea) are shown on the bottom. Although the SNR ratio ideally should normalize for dose variations, large run-to-run variability is still observed likely due to changes in polarizer/scanner transport time and polarization variations.

TABLE I

Relaxation and Polarization Measurements in Solution (B_0 = 3T, 37 °C):

	[^{13}C]urea	[^{13}C, ^{15}N$_2$]urea
T_1 (aqueous) [s]	46 ± 1	44 ± 1
T_2 (aqueous) [s]	.09 ± .01	24 ± 4
T_2 (plasma) [s]	.23 ± .01	11 ± 1
T_2 (whole blood) [s]	.24 ± .01	4.9 ± .2
Polarization at 25 s	19 ± 5%	22 ± 2%

TABLE II

T_2 Distributions *in Vivo*.

	parameter	location	mean±σ [s]	k [†]
	$T_{2,L}$	Pelvis	11.0 ± 1.8	.13 ± .09
	$T_{2,L}$	Medulla	6.28 ± 1.27	.13 ± .03
$[^{13}C, ^{15}N_2]$	$T_{2,S}$	Pelvis	1.14 ± .38	-
	$T_{2,S}$	Medulla	1.15 ±0.42	-
	$T_{2,S}$	Aorta	1.31 ± 0.34	-
$[^{13}C]$	T_2	Kidney	0.231 ± 0.026	-
	T_2	Aorta	0.279 ± 0.027	-

[†]Shape Parameter of the Frechet Distribution